

Major Classification: Biological Sciences

Minor Classification: Applied Biological Sciences

Outer membrane vesicles catabolize lignin-derived aromatic compounds in *Pseudomonas putida* KT2440

Davinia Salvachúa^{1,2,‡}, Allison Z. Werner^{1,2,‡}, Isabel Pardo^{1,‡}, Martyna Michalska^{3,‡}, Brenna A. Black⁴, Bryon S. Donohoe⁴, Stefan J. Haugen⁴, Rui Katahira¹, Sandra Notonier^{1,2}, Kelsey J. Ramirez⁴, Antonella Amore⁴, Samuel O. Purvine⁵, Erika M. Zink⁵, Paul E. Abraham^{2,6}, Richard J. Giannone^{2,6}, Suresh Poudel^{2,6}, Philip Laible³, Robert L. Hettich^{2,6,*}, Gregg T. Beckham^{1,2,*}

¹National Bioenergy Center, National Renewable Energy Laboratory (NREL), Golden, CO, USA; ²Center Bioenergy Innovation, Oak Ridge National Laboratory, Oak Ridge, TN, USA; ³Argonne National Laboratory, Lemont, IL, USA; ⁴Biosciences Center, NREL, Golden, CO, USA; ⁵Environmental Molecular Sciences Laboratory, Pacific Northwest National Laboratory, Richland, WA, USA; ⁶Oak Ridge National Laboratory, Oak Ridge, TN, USA

‡Equal contributions.

*Corresponding authors: gregg.beckham@nrel.gov; hettichrl@ornl.gov

Abstract: Lignin is an abundant and recalcitrant component of plant cell walls. While lignin degradation in nature is typically attributed to fungi, growing evidence suggests that bacteria also catabolize this complex biopolymer. However, the spatiotemporal mechanisms for lignin catabolism remain unclear. Improved understanding of this biological process would aid in our collective knowledge of both carbon cycling and microbial strategies to valorize lignin to value-added compounds. Here, we examine lignin modifications and the exoproteome of three aromatic catabolic bacteria: *Pseudomonas putida* KT2440, *Rhodococcus jostii* RHA1, and *Amycolatopsis* sp. ATCC 39116. *P. putida* cultivation on lignin-rich media is characterized by an abundant exoproteome that is dynamically and selectively packaged into outer membrane vesicles (OMVs). Interestingly, many enzymes known to exhibit activity towards lignin-derived aromatic compounds are enriched in OMVs from early to late stationary phase, corresponding to the shift from bioavailable carbon to oligomeric lignin as a carbon source. *In vivo* and *in vitro* experiments demonstrate that enzymes contained in the OMVs are active and catabolize aromatic compounds. Taken together, this work supports OMV-mediated catabolism of lignin-derived aromatic compounds as an extracellular strategy for nutrient acquisition by soil bacteria and suggests that OMVs could potentially be useful tools for synthetic biology and biotechnological applications.

Significance Statement: The valorization of the plant polymer lignin is critical to enable the bioeconomy, but the heterogeneity of lignin presents a barrier to its use. Natural microbial conversion processes funnel aromatic compound mixtures to single products, and thus have emerged as a means to overcome lignin heterogeneity. Accordingly, understanding the mechanisms that bacteria employ to convert lignin degradation products are of importance for their eventual industrial application. Here we demonstrate that a promising bacterial chassis for lignin-relevant synthetic biology, *Pseudomonas putida*, secretes outer membrane vesicles that turnover aromatic compounds extracellularly. From this work, we propose a new mechanism for extracellular nutrient acquisition from aromatic compounds by soil bacteria, which holds promise for improving the efficiency of microbial lignin conversion.

Introduction

Plant cell walls are a complex matrix of biopolymers that are highly recalcitrant to decay, mainly due to the presence of lignin (1), which is an aromatic polymer synthesized via radical coupling of monolignols (2). Given its prevalence in plants, lignin is estimated to account for 30% of Earth's non-fossil organic carbon (2). Despite the natural abundance of lignin, relatively few microbes can efficiently breakdown this biopolymer, and for many years, oxidoreductases such as laccases and peroxidases secreted by white-rot fungi were thought to be the major enzymatic actors in biological lignin depolymerization (3). However, recent work has begun to suggest an important role for bacteria in lignin conversion (4-7).

The liberated products of lignin depolymerization represent a large carbon and energy source for microbial life. To understand the fate of these compounds, the environmental microbiology community has mapped various pathways that microbes employ for the intracellular catabolism of monomeric aromatic species, motivated in part by the release of xenobiotic aromatic pollutants (8). These efforts have led to deeper understanding of the primary pathways for bacterial catabolism of lignin-derived, monomeric aromatic compounds (5, 6). Pioneering research, mainly from Masai and Fukuda, has also led to the discovery of multiple bacterial pathways for the cleavage of lignin-derived dimers (5, 6). Taken together, these studies have gained the attention of the biomass conversion research community wherein lignin conversion to valuable products is recognized as a critical need for a successful plant-based carbon economy (9-12).

Since large lignin oligomers, especially with carboxylate groups or covalently-linked glucosides, may not readily translocate across the bacterial cell membrane (13) it is commonly assumed that secreted enzymes are responsible for the extracellular depolymerization or modification of lignin. Exoproteomics studies have been conducted in a few aromatic-catabolic bacteria to investigate microbe-lignin interactions (14-16). However, these studies are few and typically do not consider spatiotemporal changes in the extracellular milieu or the compartmentalization of various biological functions. Overall, improved understanding about how microbes interact with lignin and lignin-derived compounds in the extracellular milieu would provide further insights into global carbon cycling and biological strategies to valorize lignin.

To that end, here we study the spatiotemporal interaction of three soil bacteria (*Pseudomonas putida* KT2440, *Rhodococcus jostii* RHA1, and *Amycolatopsis* sp. ATCC 39116) with a lignin-rich substrate via nuclear magnetic resonance (NMR) spectroscopy to track the lignin chemistry as a function of microbial cultivations, and exoproteomics to identify the proteins in the extracellular environment. In all three bacteria, the exoproteomes are distinct from the proteins detected in the intracellular fractions. However, the *P. putida* lignin-induced exoproteome is highly abundant and

dynamic in its protein content compared to the other organisms. This bacterium is also characterized by the abundant secretion of outer membrane vesicles (OMVs) in the presence of lignin, which are known to be implicated in a diverse set of functional roles in Gram-negative (17) (and some Gram-positive (18)) bacteria, including communication, virulence, and nutrient acquisition, among others (19, 20). We conduct further proteomics experiments which demonstrate that these OMVs dynamically encapsulate enzymes, including those in the β -ketoadipate pathway (β KA) (a central pathway to the catabolism of lignin-derived aromatics in this microbe (21)). In addition, functional assays demonstrate that isolated OMVs are involved in 4-hydroxybenzoate and protocatechuate turnover, key compounds in aromatic catabolism through the β KA pathway. Overall, this work presents a new role for OMVs in the extracellular catabolism of lignin-derived compounds by a soil microbe. The capability of OMV secretion for extracellular catabolism of toxic substrates may be an additional reason that *Pseudomonas putida* KT2440 is inherently such a robust bacterium (22). We also discuss the ability to harness OMVs as a general means to conduct enzymatic reactions extracellularly, for example to consume or produce toxic compounds, for synthetic biology applications.

Results

To explore the interaction of aromatic-catabolic bacteria with lignin, we selected a Gram-negative bacterium (*P. putida* KT2440, hereafter *P. putida*) and two Gram-positive bacteria (*R. jostii* RHA1 and *Amycolatopsis* sp. ATCC 39116, hereafter *R. jostii* and *Amycolatopsis* sp.), which we previously reported to utilize a significant amount of lignin in a soluble, lignin-rich stream compared to other aromatic-catabolic bacteria (7). The lignin-rich substrate utilized in this study is a soluble alkaline extract from corn stover, which contains aromatic monomers and oligomers (*SI Appendix*, Fig. S1) that retain β -O-4 linkages from native lignin.

We first analyzed bacterial growth and carbon utilization in lignin-rich media (i.e. aromatic compounds, carboxylic acids, and supplemental glucose) and, for comparison purposes, also in lignin-free media (containing glucose as the only carbon and energy source) over 120 h. Utilizable aromatic monomers, aliphatic carboxylic acids, and glucose were depleted within 24 h in *P. putida* cultures and within 72 h in *R. jostii* and *Amycolatopsis* sp. (Fig. 1a-c and *SI Appendix*, Fig. S2), with oligomeric lignin as the primary remaining carbon source. The initial lignin content (monomeric + oligomeric) in these cultures was 1.7 g/L and the total concentration of monomeric aromatic compounds was 0.27 g/L (16% of the total lignin) (*SI Appendix*, Table S1). Since these organisms utilized a lignin content of 23.4%, 18.9%, and 24.4% (Fig. 1a-c), as measured with our previous approach (7), it is likely that they utilized a small fraction of lignin oligomers (7.4 ± 2.1 % for *P. putida*, 2.9 ± 2.3 % for *R. jostii*, and 8.4 ± 0.2 % for *Amycolatopsis* sp. by 120 h).

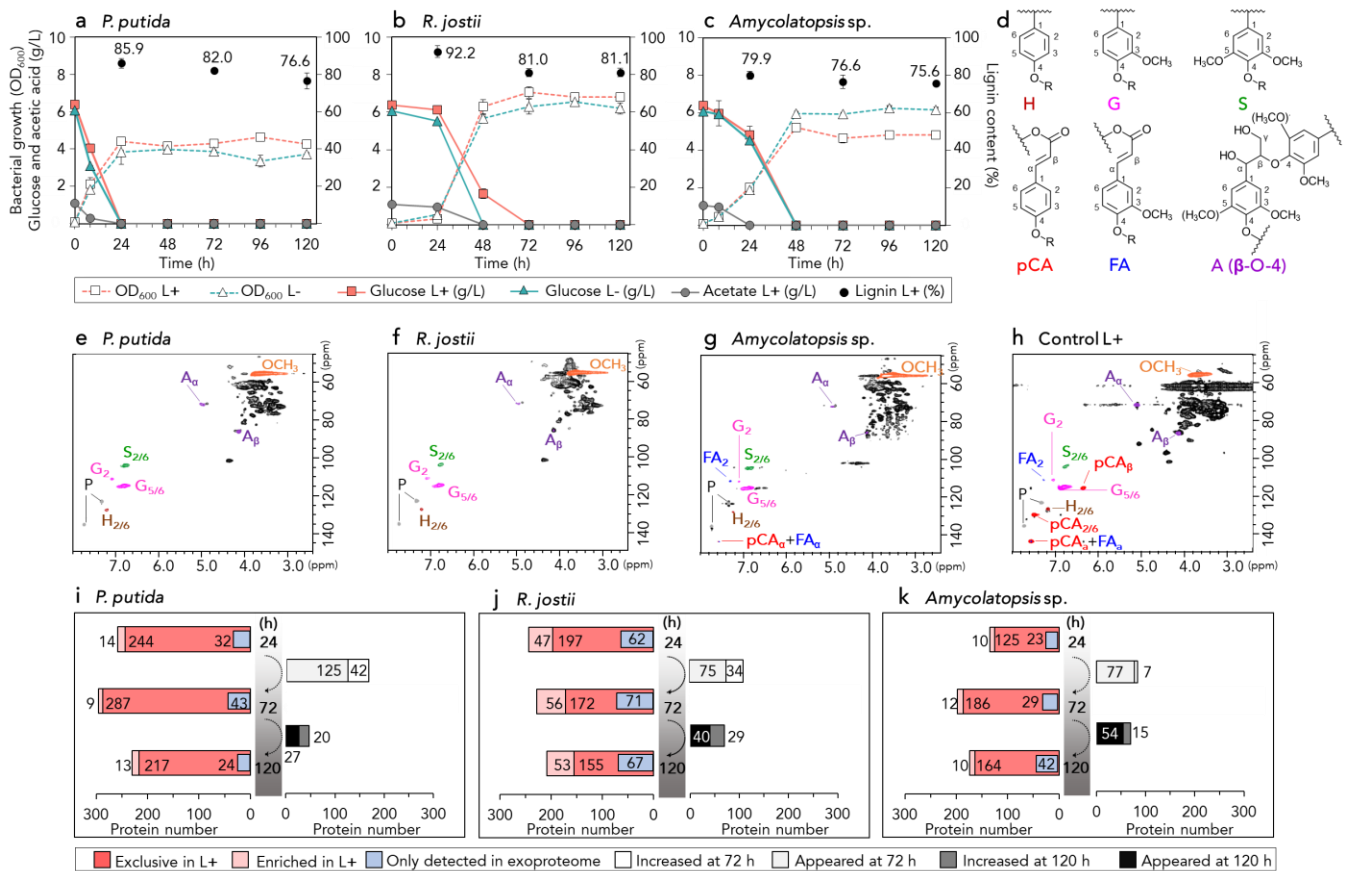


Fig. 1 | Chemical and proteomics analyses in lignin-free (L-) and lignin-rich (L+) bacterial cultures. **a-c**, Bacterial growth (OD₆₀₀) and concentrations of the major carbon sources in **a**, *P. putida*, **b**, *R. jostii*, and **c**, *Amycolatopsis* sp. cultivations. The concentrations of minor carbon sources are shown in *SI Appendix*, Fig. S2. Error bars show the absolute difference between two biological replicates. **e-h**, Structural lignin units analyzed by 2D-HSQC NMR spectroscopy in 5-day L+ cultures of **e**, *P. putida*, **f**, *R. jostii*, **g**, *Amycolatopsis* sp. and **h**, non-inoculated 5-day sample (control). Temporal and high-resolution spectra of the side chain and aromatic regions are presented in the *SI Appendix*, Figs. S3 to S6. P = pyridine (internal standard), OCH₃ = methoxy groups. **i-k**, Results from proteomic analyses in **i**, *P. putida*, **j**, *R. jostii*, and **k**, *Amycolatopsis* sp. cultures. The left side of the bar chart shows the number of exclusive (in red) and enriched (in pink) proteins in L+ cultures compared to L- cultures as well as the number of proteins from that pool of proteins that appear only in the exoproteome compared to the intracellular fraction (in blue). The right side of the bar chart shows the number of proteins that appear or increase over time (from 24-to-72 h or from 72-to-120 h) within the pool of exclusive or enriched proteins in L+ cultures. The complete list of proteins is shown in *SI Appendix*, Tables S3 to S8. These analyses originate from two biological replicates and two technical replicates in each organism, each time point (24, 72, 120 h), each media (L+, L-) and each protein location (extracellular vs intracellular). Proteins in L+ cultures whose absolute log ratios value exceeded 2 standard deviations of all log ratios within the pairwise comparison 'L+ vs L-' are denoted as 'enriched'. Proteins in 72 or 120 h cultures whose absolute log ratios value exceeded 2 standard deviations of all log ratios within the pairwise comparison '72 vs 24 h' or '120 vs 72 h', respectively, are denoted as 'increased'.

To understand the chemical changes in lignin, we also conducted 2-D-heteronuclear single quantum correlation-NMR (2D-HSQC NMR) spectroscopy as a function of time (Fig. 1d-h and *SI Appendix*, Figs. S3 to S6). This technique is commonly used to understand lignin chemistry (23, 24) including to elucidate modifications by chemical catalysts (25) and ligninolytic enzymes (26, 27). The major changes occurred from 0 to 72 h. FA₂, pCA_β, pCA_{2/6}, and pCA_α+FA_α signals disappear at 72 h in *P. putida* and *R. jostii* treatments, which corresponds to *p*-coumaric and ferulic acid depletion analyzed by LC-MS/MS (*SI Appendix*, Fig. S2). Conversely, *Amycolatopsis* sp. still exhibits signals for FA₂ and pCA_α+FA_α at 120 h, although the latter was reduced compared to the non-inoculated control. 2D-HSQC-NMR spectra also exhibit a reduction in the A_α and A_β signals from the β-O-4 bond in the three bacteria compared to the control, which suggests that these bacteria are breaking down oligomeric lignin. However, it is worth noting that this cleavage does not necessarily imply increased lignin utilization.

To provide insights into the extracellular enzymes potentially involved in lignin catabolism, we conducted differential (lignin-free and lignin-rich media), spatial (intracellular and extracellular), and temporal (24, 72, and 120 h of incubation) proteomic analyses with the three bacteria (*SI Appendix*, Excel S1). *P. putida* reached stationary phase at 24 h and *R. jostii* and *Amycolatopsis* sp. between 48-72 h, when most of the readily available carbon sources were depleted (Fig. 1a-c). Despite reaching stationary phase – a growth phase that leads to cell lysis events – the percentage of differential proteins between the extracellular and intracellular fractions was 54, 33, and 60% in *P. putida*, *R. jostii*, and *Amycolatopsis* sp., respectively (*SI Appendix*, Fig. S7), indicating that the intracellular and extracellular fractions are different. The extracellular fraction contained a less diverse set of proteins compared to the intracellular fraction in all cases, and *P. putida* exhibited the highest number of lignin-induced extracellular proteins compared both to the intracellular fraction and the other organisms (Fig. 1i-k and *SI Appendix*, Fig. S8). It is notable that the other microbes

exhibit a higher number of predicted proteins from the genome than *P. putida* (*SI Appendix*, Table S2). Furthermore, the *P. putida* exoproteome showed that a higher number of proteins were enriched when oligomeric lignin became the major carbon source (from 24 to 72 h) compared to the other two organisms (from 72 to 120 h) (Fig. 1i-k).

To identify putative enzymes that could be involved in lignin modification and/or depolymerization from these large pools of proteins, here we focused on lignin-induced extracellular proteins that were not detected in the intracellular compartment (*SI Appendix*, Fig. S9). The most represented catalytic functions, according to gene ontology (GO) annotation, were hydrolases and oxidoreductases in the three organisms (~30-40%) (*SI Appendix*, Tables S3 to S5). Notably, these functions were further enriched in the subset of proteins that appeared or increased at the time at which oligomeric lignin was the major carbon source – up to 56% in *P. putida* and 80% in *Amycolatopsis* sp. (the percentages remained similar in *R. jostii*, ~40%) (*SI Appendix*, Table S6 to S8). Most of the lignin-depolymerizing enzymes described to date, including some potentially involved in β -O-4 cleavage (i.e. dye decolorizing peroxidases (DyPs) (28-30), multicopper oxidases (31, 32)) belong to the broad group of oxidoreductases. In the current analysis, we have only detected a DyP in *P. putida*. However, we also found other enzymes which could be potentially involved in the modification of both oligomeric and monomeric aromatic or phenolic compounds (*SI Appendix*, Tables S3 to S8). For instance, azoreductases (33, 34), a xenobiotic reductase (35), and a 2,3-quercetin dioxygenase (36) were detected in *P. putida*. All but DyP appeared or were enriched when oligomeric lignin was the major carbon source. In the case of *R. jostii*, a cholesterol oxidase (37) and a cytochrome P450 (38) were also observed. In *Amycolatopsis* sp., another cholesterol oxidase, cytochrome P450, and two oxidoreductases (one potentially belonging to the glucose-methanol-choline (GMC) superfamily) (39) were detected. Among these enzymes, only the cytochrome P450 in *R. jostii* and cholesterol oxidase in *Amycolatopsis* sp. appeared from 72 and 120 h, when oligomeric lignin is the major remaining carbon source (see protein access numbers in *SI Appendix*, Tables S3 to S8). Additional information on these oxidoreductases, as well as other enzymes that were not part of this protein subset and that are potentially involved in lignin modification, is presented in *SI Appendix*, Text S1.

A question that arises from these data is how the various proteins are transported from the cell to the extracellular

milieu. We employed several algorithms (i.e. SignalP, TatP, SecP, PSORTb) to predict protein location or export from the cytoplasm (40-43). Only 40% of the lignin-induced proteins (that were exclusively detected in the extracellular fraction) were predicted to be extracellular and/or exported in *P. putida* by at least one of the algorithms, whereas 70% in *R. jostii* and *Amycolatopsis* sp. are predicted to be secreted (*SI Appendix*, Tables S9 to S11). Moreover, a larger number of lignin-induced proteins in the exoproteome of *P. putida* lignin cultures are predicted to participate in catabolic (32-37 proteins) and biosynthetic processes (74-89 proteins) compared to *R. jostii* (10-16 and 25-33 proteins) and *Amycolatopsis* sp. (5-13 and 20-40 proteins) (*SI Appendix*, Figs. S10 to S12). Interestingly, some enzymes from the β KA pathway (considered to be cytoplasmic) were detected in the extracellular fraction of *P. putida* and *R. jostii* in lignin cultures and to a lower extent in *Amycolatopsis* sp. (*SI Appendix*, Text S2 and Figs. S13 to S18 show detailed trends in both intracellular and extracellular fractions for the β KA pathway and alternative routes for the catabolism of aromatics). Taken together, these results highlight the importance of considering other enzyme secretion mechanisms that cannot be predicted by these algorithms or explained due to cell lysis.

Based on these results, we performed electron microscopy to investigate cell integrity and the response to the lignin-rich substrate. Interestingly, we observed that *P. putida* secretes a striking amount of OMVs in lignin-rich media (Fig. 2a-b) especially when compared to *P. putida* in lignin-free media or *R. jostii* and *Amycolatopsis* sp. in either media (*SI Appendix*, Fig. S19). In view of these observations, we hypothesized that some of the proteins not predicted to be secreted could be trafficked to the extracellular compartment via OMVs. Thus, we next focused on *P. putida* OMVs. While the production of OMVs by this bacterium has been previously described (44), their interaction with lignin has not yet been reported. Dynamic light scattering (DLS) measurements and transmission electron microscopy (TEM) (Fig. 2e-f) identified two distinct sizes of OMVs in both media formulations with no clear trend in vesicle diameter over time (Fig. 2c-d). A 7% increase in cell death is observed in lignin-rich media compared to lignin-free media (*SI Appendix*, Fig. S20), which may contribute to production of vesicles via explosive cell lysis (17). Regardless, both scanning electron microscopy (SEM) and TEM data confirm that OMVs are also secreted via blebbing events from the outer membrane of *P. putida* cells with undamaged membranes even in late stationary phase (Fig. 2g-h).

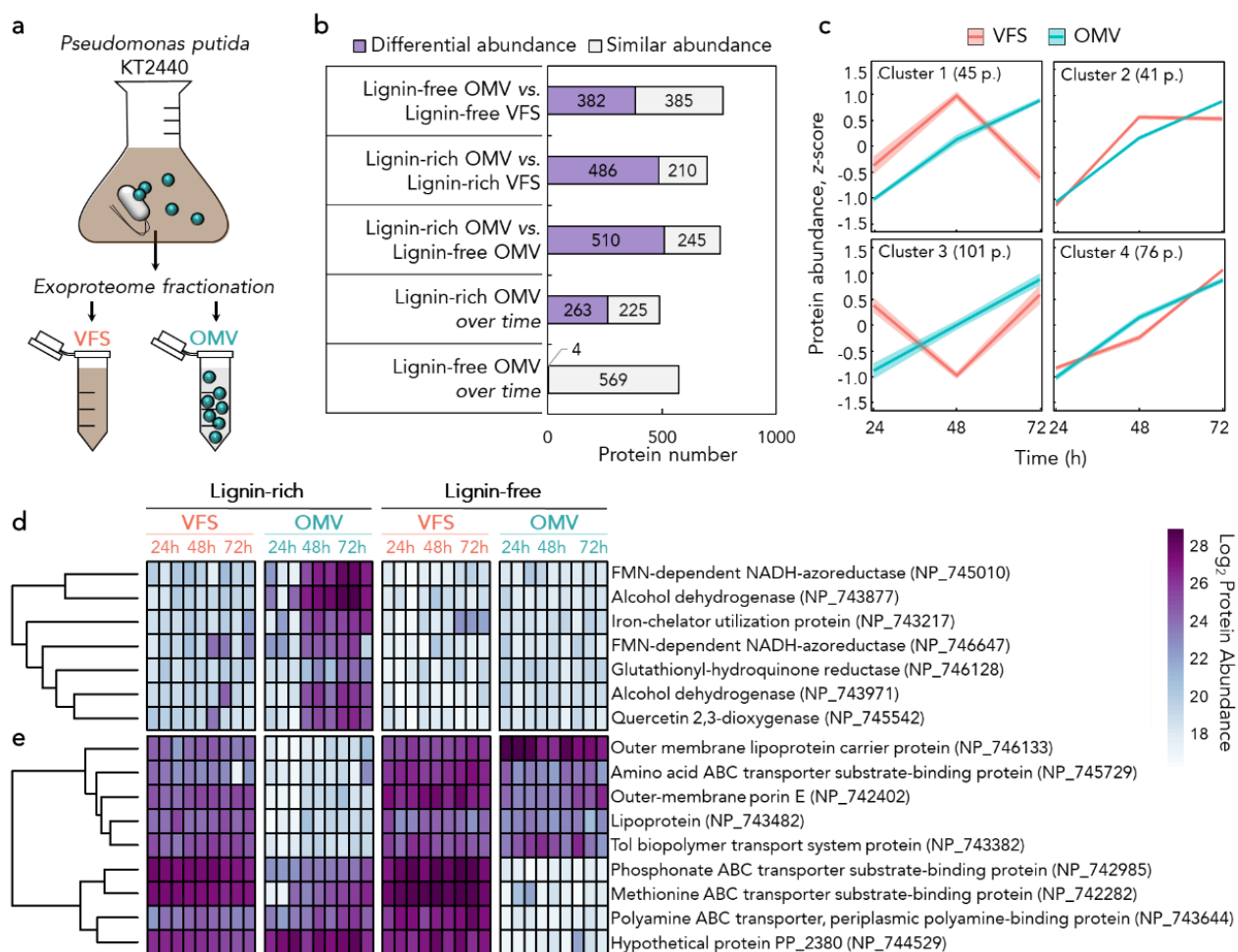


Fig. 3 | The exoproteome is selectively compartmentalized into OMVs and the protein content of OMVs from lignin-rich cultivations is highly dynamic over time. **a**, The extracellular milieu (=exoproteome) was fractionated into outer membrane vesicles (OMVs) and vesicle-free secretome (VFS) prior to proteomics analysis of each fraction from biological triplicates grown in lignin-rich and lignin-free media at 24, 48, and 72 h of cultivation. **b**, Proteins with differential abundance between the OMV and VFS, or OMV over time. Tests were conducted with a pairwise ANOVA on data from biological triplicates and a Benjamini-Hochberg correction was performed on the resulting *p*-values; proteins which had a *p*-value < 0.05 are considered to have differential abundance and those which did not meet this significance cut-off are considered to have similar abundance. Proteins with differential abundance between each time-point in lignin-rich OMVs are presented in *SI Appendix*, Table S14. **c**, Temporal trends of abundance in the OMV and VFS for the 263 proteins that change over time in lignin-rich OMVs. Clusters were identified by *k*-means clustering and protein abundance is presented as a z-score. Trend lines represent the 95% confidence interval for VFS proteins (red) and OMV proteins (blue) in each cluster. The number of proteins in each cluster are presented in the upper left-hand corner and listed individually in *SI Appendix*, Table S13. **d-e**, Heat-mapped log₂ protein abundance for select proteins for each biological triplicate at 24, 48, and 72 h of cultivation in the VFS and OMV in lignin-rich and lignin-free media. NCBI RefSeq identifiers are provided for each protein in parentheses following the description. **d**, Select proteins with enrichment into lignin-rich OMVs and function (known or putative) in oxidation-reduction processes. **e**, Select proteins with differential abundance between lignin-rich and lignin-free OMVs and function (known or putative) as a lipoprotein, small-molecular binding protein, transport-related, or OMP.

Next, we examined enzymes from the β KA pathway (Fig. 4a) as they were detected in previous exoproteome analysis (*SI Appendix*, Fig. S14). Of the detected proteins in the β KA pathway, all are strongly enriched in the OMVs from lignin-rich media compared to the VFS and the lignin-free exoproteome (Fig. 4b). Intra-OMV abundance of β KA enzymes increases temporally after 24 h of cultivation (Fig. 4b). Since enrichment is not observed in the VFS, we posit that enzymes in the β KA pathway are secreted via OMVs for the extracellular turnover of lignin-derived aromatics.

To test this hypothesis, we engineered two *P. putida* deletion mutants that cannot grow on two catabolic intermediates: *P. putida* Δ *pobAR* on 4-hydroxybenzoate (4-HBA) and *P. putida* Δ *pcaHG* on protocatechuate (PCA). These mutants were inoculated to the same cell density and separately

complemented with wild-type OMVs for growth analyses (*SI Appendix*, Fig. S25 and Table S15). A boiled OMV control was also included to test if incorporated or encapsulated metabolites (e.g., lipids, amino acids) complement growth. Boiled OMVs enhance growth (OD₆₀₀ after 72 h) of *P. putida* Δ *pobAR* by 175% and *P. putida* Δ *pcaHG* by 153% (Fig. 4c). Active OMVs enhance growth of *P. putida* Δ *pobAR* cultivations on 4-HBA by 336% and *P. putida* Δ *pcaHG* cultivations on PCA by 319% (Fig. 4c). While these growth enhancements are roughly double to what is observed in the boiled control, active OMV complementation does not fully restore the growth observed in wild-type cultivations (*SI Appendix*, Fig. S26 and Table S15), suggesting a limited enzyme content, lifetime in the exoproteome, and/or lack of co-factors.

To further test the hypothesis that OMVs mediate aromatic catabolism, we tested *in vitro* turnover of 4-HBA and PCA by OMVs. PCA is known to be unstable, which was reflected in the 24% and 27% turnover in abiotic and boiled controls, respectively (Fig. 4d and *SI Appendix*, Fig. S27). Interestingly, active OMVs increase the turnover of PCA by 59%, demonstrating PcaHG remains catalytically active into the OMVs (Fig. 4d). Conversely, 4-HBA turnover is not improved by active OMVs (Fig. 4d). It is noteworthy that PobA requires NADPH as a co-substrate whereas PcaHG

does not (Fig. 4a). Considering NAD(P)H instability, its content in isolated OMVs remains unknown. In fact, when OMVs were provided exogenous reducing equivalents, NAD(P)H only decreased in the presence of 4-HBA (*SI Appendix*, Fig. S28). While this does not provide information on the *in vivo* presence of NAD(P)H or the generation thereof, these results indicate that PobA activity is retained inside the OMV. Together, these data demonstrate that OMV-encapsulated enzymes actively contribute to the turnover of model lignin-derived aromatic compounds.

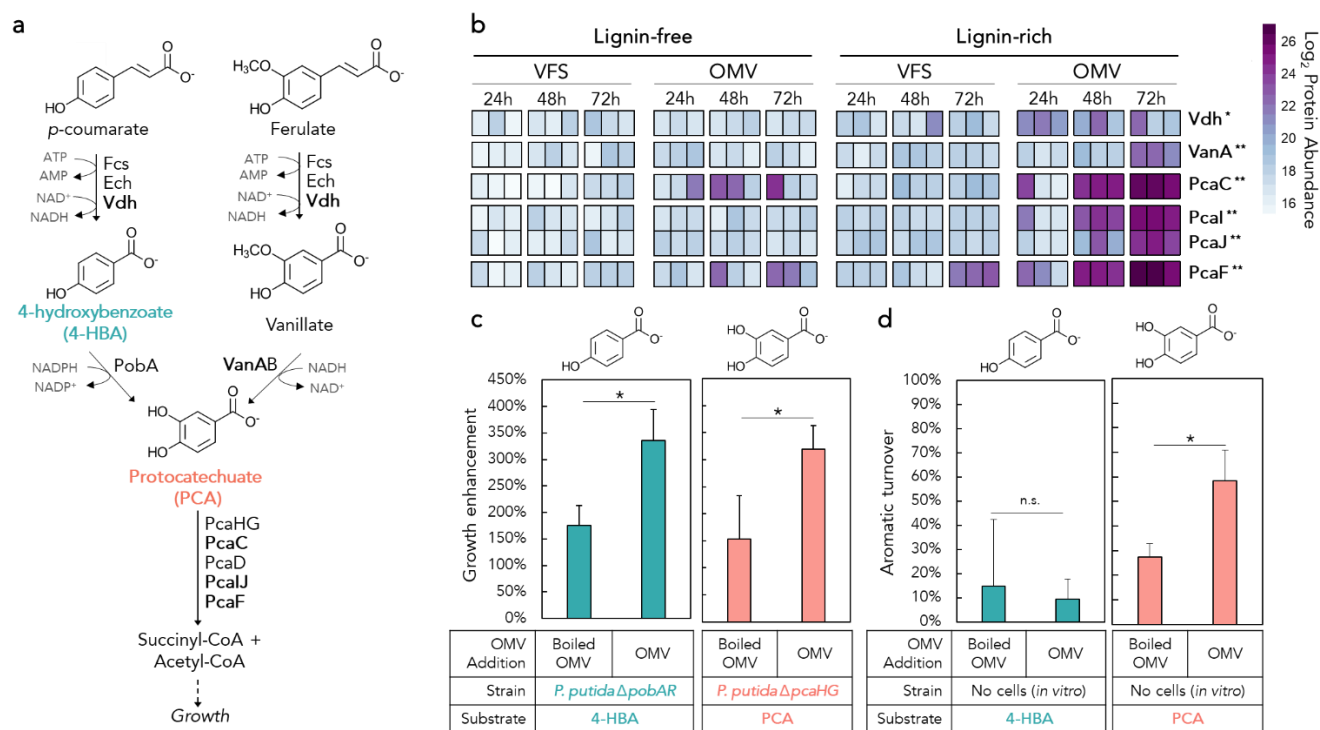


Fig. 4 | Catabolism of lignin-derived aromatics via the β -ketoadipate pathway is enhanced by OMVs. **a**, The β -ketoadipate (BKA) pathway for catabolism of lignin monomers *p*-coumarate and ferulate into succinyl-CoA and acetyl-CoA, which support cellular growth. Metabolites which were used for *in vivo* and *in vitro* assays are shown in blue and orange color. Proteins in bold were detected in the proteomics analysis. Due to the non-targeted proteomics methodology employed throughout this study, we note that lack of detection of certain enzymes from the β KA pathway does not necessarily mean biological absence. **b**, Proteins detected within the β -ketoadipate pathway in the VFS or OMV plotted as a heat map of log₂ abundance. Values for biological triplicate at each time point are plotted separately. **p*<0.05 and ***p*<0.005 from an ANOVA with Tukey's HSD of the VFS relative to OMV. **c**, Improvement of final culture growth (OD₆₀₀) from complementation of *P. putida* Δ pobAR or *P. putida* Δ pcaHG with wild-type OMVs (boiled or fresh) for growth on M9 minimal media with 4-hydroxybenzoate (4-HBA) or protocatechuate (PCA), respectively, as the sole carbon and energy source. Growth enhancement was calculated as the percent increase in OD₆₀₀ from the mutant strain + substrate to the mutant strain + substrate + OMV. **p*<0.05 from a one-tailed paired *t*-test. **d**, *In vitro* turnover of 4-HBA or PCA by boiled or fresh OMVs. Values are displayed as the percent decrease in substrate from *t*=0 h to *t*=24 h of incubation. **p*<0.05 and n.s.=*p*>0.05 from a one-tailed paired *t*-test.

Discussion

The discovery of extracellular compartmentalization of aromatic-catabolic and putatively ligninolytic enzymes provides new insights into microbial lignin conversion. In 2015, we observed that the three bacteria (among 15) studied in this work were top performers in terms of lignin conversion (7). Using these three bacteria, here we quantify the fraction of oligomeric lignin that is utilized, propose that lignin breakdown occurs via β -O-4 bond cleavage based on 2-D HSQC NMR spectroscopy, and highlight a variety of oxidoreductases and other proteins from exoproteomics data that are worthy of further study to understand bacterial lignin catabolism. Furthermore, we report the spatial sub-compartmentalization and temporal dynamics of the exoproteome in *P. putida*, underscoring the importance of considering OMVs to understand bacteria-lignin interactions. In the case of *P. putida*, OMV production has

been previously reported to be a response to various environmental stressors and showed media-dependent protein cargo (44, 47, 48). Our results expand upon these previous studies by demonstrating temporal cargo sorting of relevant enzymes into OMVs to enhance the extracellular catabolism of lignin-derived aromatic compounds.

Based on this work, we propose a model for OMV-mediated lignin conversion and nutrient acquisition (Fig. 5). In this model, first, OMVs are secreted with an encapsulated, functional set of proteins. Substrate turnover could then occur intra-OMV to enable protected enzyme activity and/or cofactor maintenance, followed by cellular uptake of released products (Fig. 5a) or OMV delivery to the cell (Fig. 5b) as has been previously reported (49, 50). Alternatively, the OMV may lyse to allow direct enzymatic access to large

substrates and extracellular substrate turnover, followed by product uptake by the cell (Fig. 5c).

A key limitation of the current study is that we demonstrate functional OMV assays only for aromatic monomers, but not for lignin oligomers. While the model presented in Fig. 5 serves to explain the results obtained with monomeric lignin-derived compounds, it could also be applicable to the degradation of oligomeric lignin (see Fig. 5c). Among others, a challenge to test this model with lignin oligomers and polymers is the difficulty of attributing lignin depolymerization exclusively to enzymes, since abiotic processes can also be involved (51). Additionally, cofactor presence and regeneration in OMVs, which would be a requirement for sustained conversion of aromatic compounds and lignin oligomers, also remains challenging to study. Namely, the detection and tracking of unstable compounds such as NAD(P)H and ATP is currently hindered by OMV isolation conditions.

To test and refine the model in Fig. 5, additional studies are required to interrogate OMV lifetime, metabolite import and export from OMVs, and OMV-cell fusion events. An important, outstanding question relates to the extent of extracellular carbon turnover by the OMVs relative to intracellular turnover. To address this question, spatially-resolved fluxomics, which was recently developed and applied to exosomes (52, 53) and quantitative proteomics of the β KA pathway will be key to understanding the spatial distribution of aromatic catabolism (extracellular versus intracellular) *in vivo*. Another interesting observation from the current study is the size heterogeneity of OMVs, which potentially suggests functional specialization and different routes for OMV biogenesis. Recent work employing asymmetric flow field flow fractionation to separate vesicles by size discovered distinct protein and lipid profiles attributed to exosome subpopulations (54), revealing a layer of complexity that remains to be explored in bacterial OMVs.

This work demonstrates that OMVs harbor functional aromatic catabolic enzymes, but the evolutionary and

physiological driver for use of OMVs in this context remains unknown. OMV production may benefit *P. putida* KT2440 and other bacteria that deploy OMVs by providing a means to access nutrient sources that cannot translocate the cell membrane and/or mitigate substrate toxicity (both intrinsic and generated through metabolic intermediates) (55) by restricting cytoplasmic encounters or by modifying toxic compounds to less toxic molecules extracellularly, thus increasing strain fitness. *P. putida* KT2440 is derived from *P. putida* mt-2, which is studied for its remarkable capability to degrade toluene and other toxic pollutants (56, 57). The general metabolic versatility (58) and robust toxicity tolerance (22, 59) attributed to Pseudomonads has inspired widespread adoption of domesticated *P. putida* for biotechnology and bioremediation (60, 61). Future exploration of the role of OMVs in *P. putida* KT2440 may serve to provide direct insights into how OMVs contribute to microbial robustness in toxic environments.

Going forward, OMV-mediated secretion of biological components for extracellular biocatalysis can also be considered as a synthetic biology tool. Engineered packaging of specific enzymes into OMVs has been demonstrated via bioconjugation to OmpA (62). Protein scaffolding is an interesting possibility for OMV-mediated secretion of functional sets of enzymes, both as a means to explain the natural phenomena of coordinated protein secretion in the absence of identifiable secretion tags, and as an engineering tool (63). Encapsulation and secretion of enzymes via OMVs could also serve to protect cargo from proteolysis (64), enable long-distance delivery of proteins or other biological materials (65), enhance the tolerance for the utilization or production of toxic compounds of interest in engineered strains, and promote extracellular digestion of complex substrates (66-68). Overall, the current work shows that focus is needed to understand how OMVs are employed in carbon cycling and for conversion of waste organic carbon into valuable chemical products as well as to exploit bacterial OMVs for biotechnological applications.

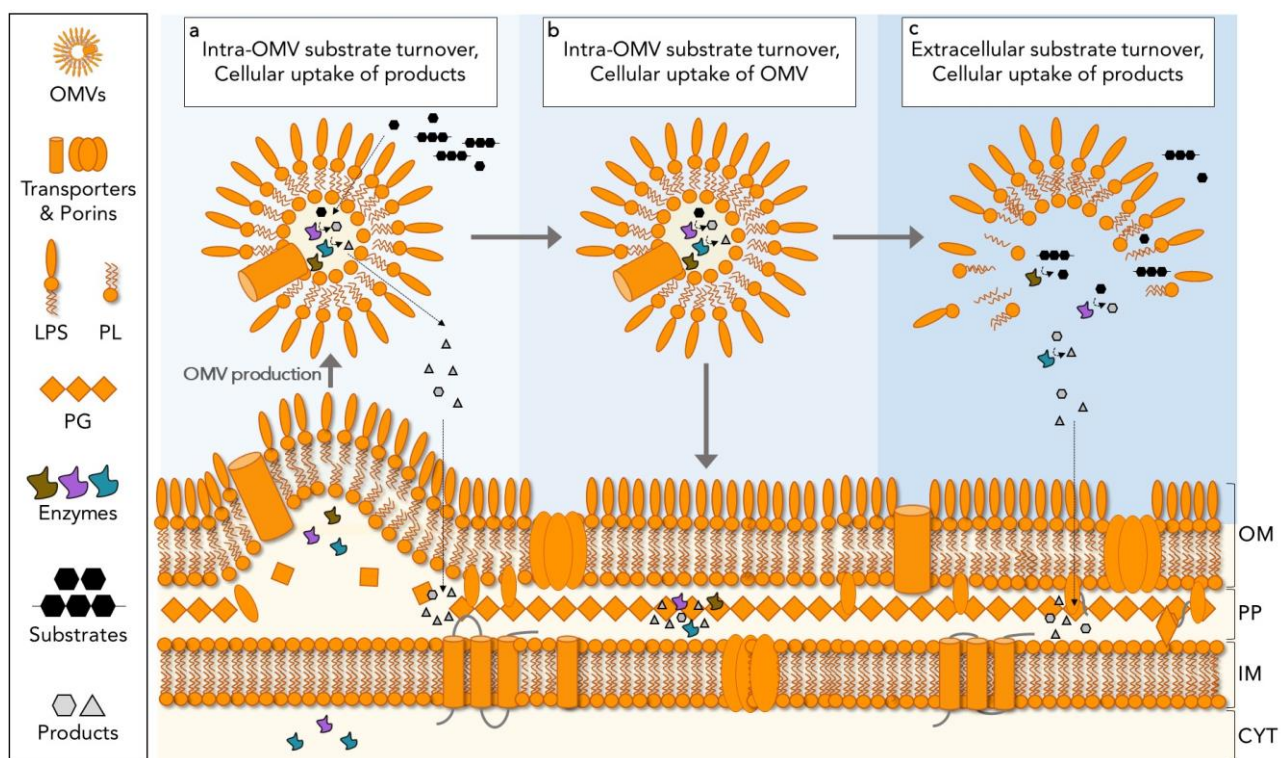


Fig. 5 | Model for OMV-mediated nutrient acquisition and/or catabolism of toxic substrates in *P. putida*. A functional set of enzymes are secreted to the extracellular milieu via OMVs in response to a nutrient source, such as lignin-derived compounds. Substrates can then be catabolized inside OMVs, which may require active uptake. Cellular access to the resulting products could then occur via **a**, uptake of free products released from the OMV or **b**, direct uptake of OMVs which would contain encapsulated products. **c**, Alternatively, secreted vesicles could lyse and release the enzyme cocktail into the extracellular milieu for direct access to large substrates, such as lignin. In this scenario, uptake of products would occur as in **a**. Abbreviations: LPS: Lipopolysaccharide; PL: phospholipid; PG: peptidoglycan; OM: outer membrane; PP: periplasm; IM: inner membrane; CYT: cytoplasm.

Methods

A brief materials and methods section is presented here. See *SI Appendix*, SI Methods section for further details.

Bacterial cultivations

Pseudomonas putida KT2440 (ATCC 47054), *Rhodococcus jostii* RHA1 (generously provided by Dr. Lindsay Eltis at the University of British Columbia), and *Amycolatopsis* sp. (ATCC 39116) were inoculated at an OD_{600} of 0.1 in M9 Minimal Media with 5 g/L glucose (lignin-free cultivations) and incubated at 30°C and 225 rpm. Lignin-rich cultivations contained the same media plus additional 25% (v/v) soluble alkaline lignin from corn stover (prepared as previously described) (55).

Cell viability analyses

Samples from *P. putida* cultivations were diluted in Tris-buffered Saline (TBS), stained with LIVE/DEAD® BacLight™ (Invitrogen, L7012) per manufacturer instructions, and fluorescence was measured with 525/540 and 610/620 bandpass filters on a CytoFLEX flow cytometer (Beckman Coulter Life Sci.). Percentages of live and dead cells were calculated after appropriate gating.

Strain engineering in *P. putida* KT2440

The genetically modified *P. putida* KT2440 strains utilized in this work, $\Delta pcaHG$ (=CJ072) and $\Delta pobAR$ (=CJ182), were constructed as described previously (69).

OMV characterization

Outer membrane vesicle isolation

OMV enrichment was prepared from 0.2 μm vacuum filter clarified *P. putida* KT2440 supernatant using the ExoBacteria™ kit (SBI, #EXOBAC100A) ion exchange protocol following manufacturer instructions.

Dynamic light scattering

Enriched OMVs were analyzed in a Dyna Pro Plate Reader (Wyatt) by detecting scattered photons at 158°. The hydrodynamic diameter was calculated by fitting the autocorrelation function with medium refractive index of 1.33 and medium viscosity of 1.019 cp.

Scanning electron microscopy

Samples from bacterial cultivations were plated on poly-L-lysine coated glass coverslips, fixed with glutaraldehyde, dehydrated in increasing concentrations of ethanol, critical point dried, coated in Ir, mounted, and imaged with a FEI Quanta 400 FED SEM under 0.45 torr and beam accelerating voltage of 30 keV.

Transmission electron microscopy

Enriched OMVs were drop cast onto a glow discharged carbon file 200 mesh copper grid, and stained. *P. putida* cultivations were preserved with high-pressure freeze substitution, embedded, sectioned, and stained. Images were acquired with a 4 mega-pixel Gatan UltraScan 1000 camera on a FEI Tecnai G2 20 Twin 200 kV LaB6.

OMV assays

OMV Complementation assays

OMVs were enriched from *P. putida* KT2440 lignin-rich cultivations at 72 h. An aliquot of OMVs was heated to 100°C for >1 h and used as a boiled control. OMVs were added to washed *P. putida* $\Delta pcaHG$ or *P. putida* $\Delta pobAR$ cultivations in M9 minimal media with 10 mM protocatechuic acid or 10 mM 4-hydroxybenzoic acid, respectively, and incubated at 30°C and 225 rpm. CFUs were measured on Lysogeny Broth agar plates. OD_{600} was measured using a FLUOstar Omega plate reader.

OMV in vitro assays

OMVs were enriched from *P. putida* lignin-rich cultivations at 72 h, ultracentrifuged at 150,000g to pellet vesicles, resuspended in PBS, and incubated with 2 mM protocatechuic acid or 2 mM 4-

hydroxybenzoic acid at 30°C, 225 rpm. Samples for metabolite analysis were quantified by LC-MS/MS.

NAD(P)H consumption assays

OMVs were enriched from *P. putida* lignin-rich cultivations at 72 h, proteins were extracted, and absorbance at 340 nm was measured in the presence of a combination of 1 mM 4-hydroxybenzoate (pH 7.0), 250 µM NADH, and/or 250 µM NADPH immediately after addition of proteins for 600 s.

Lignin and metabolite analyses

Gel permeation chromatography (GPC)

GPC of soluble alkaline lignin from corn stover was conducted as previously described for lignin molecular weight analysis (26).

Compositional analysis

The bacterial supernatants from lignin-rich medium were freeze-dried and lignin content analyzed as previously described in NREL LAP/TP-510-42618 (70).

2D HSQC NMR

The bacterial supernatants from lignin-rich medium were lyophilized, ball-milled, suspended in d6-DMSO/d5 pyridine (4:1, v/v), sonicated, and spectra were acquired on a Bruker Avance III 600 MHz spectrometer at 11.7 T using a TCI probe.

Metabolite quantification: aromatic compounds, glucose, and carboxylic acids

Aromatic compounds in the lignin-rich supernatant were analyzed by electrospray ionization (ESI) liquid chromatography (LC) mass spectrometry (MS/MS) on an Ion Trap SL (Agilent) as previously described (26). Glucose and small acids in the culture supernatants were analyzed by LC-refractive index detector (RID)/UV on a Agilent 1200 LC system as previously described (71). Aromatic compounds in the OMV *in vitro* assays were analyzed by ESI-LC-MS/MS on a 6470 Triple Quadrupole Mass Spectrometer (Agilent) with multiple reaction monitoring (MRM) for each analyte.

Proteomics analyses

Intracellular and extracellular proteomics in the three bacteria species

Samples from bacterial cultivations were fractionated into cell pellets and supernatants, processed, and flash-frozen. Proteins were denatured, concentrated, extracted with chloroform:methanol as previously described (72), dried, denatured, digested with trypsin, and desalted. Peptides were detected on a Velos Pro Orbitrap Mass Spectrometer (ThermoScientific). MS/MS data search, peptide quantitation, and data analysis are detailed in *SI Appendix*.

OMV and vesicle free secretome (VFS) proteomics from *P. putida* KT2440

Supernatants from bacterial cultivations were fractionated in OMV and VFS using the ExoBacteria™ kit, flash-frozen, concentrated, washed, denatured, extracted with chloroform:methanol:water, dried, digested with trypsin, and desalted. Peptides were detected on a Q Exactive Plus Mass Spectrometer. MS/MS data search, peptide quantitation, and data analysis are detailed in Supplementary Information.

Data availability

Proteomics data from *P. putida*, *R. jostii*, and *Amycolatopsis* sp. MassIVE accession MSV000084524; ProteomeXchange accession PXD016114; Ftp connection info (only valid while private); Site: massive.ucsd.edu; Username: MSV000084524; Password: OMV.

Proteomics data from *P. putida* OMV and VFS. MassIVE accession: MSV000084506. Username: MSV000084506_reviewer. Password: OMV.

Acknowledgements

This work was authored in part by Alliance for Sustainable Energy, LLC, the manager and operator of the National Renewable Energy Laboratory for the U.S. Department of Energy (DOE) under Contract No. DE-AC36-08GO28308. Funding for the time-resolved exoproteomics efforts was provided by the U.S. DOE, Office of

Energy Efficiency and Renewable Energy, Bioenergy Technologies Office. The isolation and proteomics study of the OMVs and OMV assays were funded by The Center for Bioenergy Innovation, a U.S. DOE Bioenergy Research Center supported by the Office of Biological and Environmental Research in the DOE Office of Science. The exoproteomics of the three bacteria was done at EMSL (grid.436923.9), a DOE Office of Science User Facility sponsored by the Office of Biological and Environmental Research. Portions of the microscopy and light scattering work were supported in part by Laboratory Directed Research and Development (LDRD) funding from Argonne National Laboratory, provided by the Director, Office of Science, of the U.S. DOE under Contract No. DE-AC02-06CH11357. Use of the Center for Nanoscale Materials, an Office of Science user facility, was supported by the U.S. DOE, Office of Science, Basic Energy Sciences, under the same contract. We thank Christopher W. Johnson and Payal Khanna for sharing the *Pseudomonas putida* deletion strains. We thank Darren Peterson and David Brandner for providing the alkaline pretreated lignin liquor. We thank Samantha Peters and Payal Chirania for their assistance in proteomic sample preparation at ORNL. We thank Adam Guss for providing materials and laboratory space to conduct part of this work at ORNL. We thank Gregory A. Tira for support of initial *P. putida* OMV-characterization experiments at ANL. We thank Therese Clauss and Rosey Chu at EMSL for help with the proteomics measurements.

Author contributions

Designed experiments: DS, AZW, IP, MM, BSD, SOP, PEA, RJG, PL, RLH, GTB; Conducted experiments: DS, AZW, IP, MM, BAB, BSD, SJH, RK, SN, KJR, AA, SOP, EMZ, PEA, RJG, SP; Analyzed data: DS, AZW, IP, MM, BAB, BSD, RK, KJR, AA, SOP, PEA, RJG, SP, PL, RLH, GTB; Wrote the manuscript (which was edited and approved by all authors): DS, AZW, IP, GTB.

Competing interests

The authors declare no competing interests.

References

1. Floudas D, *et al.* (2012) The Paleozoic origin of enzymatic lignin decomposition reconstructed from 31 fungal genomes. *Science* 336(6089):1715-1719.
2. Boerjan W, Ralph J, & Baucher M (2003) Lignin biosynthesis. *Annu Rev Plant Biol* 54:519-546.
3. Martinez AT, *et al.* (2005) Biodegradation of lignocellulose: microbial, chemical, and enzymatic aspects of the fungal attack of lignin. *Int Microb* 8:195-204.
4. Masai E, Katayama Y, & Fukuda M (2007) Genetic and biochemical investigations on bacterial catabolic pathways for lignin-derived aromatic compounds. *Biosci Biotechnol Biochem* 71(1):1-15.
5. Bugg TD, Ahmad M, Hardiman EM, & Rahmanpour R (2011) Pathways for degradation of lignin in bacteria and fungi. *Nat Prod Rep* 28(12):1883-1896.
6. Kamimura N, *et al.* (2017) Bacterial catabolism of lignin-derived aromatics: New findings in a recent decade: Update on bacterial lignin catabolism. *Environm Microbiol Rep* 9:679-705.
7. Salvachúa D, Karp EM, Nimlos CT, Vardon DR, & Beckham GT (2015) Towards lignin consolidated bioprocessing: simultaneous lignin depolymerization and product generation by bacteria. *Green Chem* 17:4951-4967.
8. Fuchs G, Boll M, & Heider J (2011) Microbial degradation of aromatic compounds - from one strategy to four. *Nat Rev Microbiol* 9(11):803-816.
9. Ragauskas AJ, *et al.* (2014) Lignin valorization: improving lignin processing in the biorefinery. *Science* 344:1246843.
10. Bugg TDH & Rahmanpour R (2015) Enzymatic conversion of lignin into renewable chemicals. *Curr Opin Chem Biol* 29:10-17.
11. Beckham GT, Johnson CW, Karp EM, Salvachúa D, & Vardon DR (2016) Opportunities and challenges in biological lignin valorization. *Curr Opin Biotechnol* 42:40-53.

12. Becker J & Wittmann C (2019) A field of dreams: Lignin valorization into chemicals, materials, fuels, and health-care products. *Biotechnol Adv* 37(6):107360.
13. Vermaas JV, *et al.* (2019) Passive membrane transport of lignin-related compounds. *PNAS*:201904643.
14. Lin L, *et al.* (2016) Systems biology-guided biodesign of consolidated lignin conversion. *Green Chem* 18:5536-5547.
15. Li X, *et al.* (2019) Discovery of potential pathways for biological conversion of poplar wood into lipids by co-fermentation of Rhodococci strains. *Biotechnol Biofuel* 12:60.
16. Kumar M, *et al.* (2018) Genomic and proteomic analysis of lignin degrading and polyhydroxyalkanoate accumulating β -proteobacterium *Pandoraea* sp. ISTKB. *Biotechnol Biofuel* 11(1):154.
17. Schwachheimer C & Kuehn MJ (2015) Outer-membrane vesicles from Gram-negative bacteria: biogenesis and functions. *Nat Rev Microbiol* 13:605-619.
18. Brown L, Wolf JM, Prados-Rosales R, & Casadevall A (2015) Through the wall: extracellular vesicles in Gram-positive bacteria, mycobacteria and fungi. *Nat Rev Microbiol* 13:620-630.
19. Jan AT (2017) Outer Membrane Vesicles (OMVs) of gram-negative bacteria: A perspective update. *Front Microbiol* 8:1-11.
20. Toyofuku M, Nomura N, & Eberl L (2019) Types and origins of bacterial membrane vesicles. *Nat Rev Microbiol* 17:13-24.
21. Harwood CS & Parales RE (1996) The beta-ketoadipate pathway and the biology of self-identity. *Annu Rev Microbiol* 50:553-590.
22. Chavarría M, Nikel PI, Pérez-Pantoja D, & de Lorenzo V (2013) The Entner-Doudoroff pathway empowers *Pseudomonas putida* KT2440 with a high tolerance to oxidative stress. *Environm Microbiol* 15(6):1772-1785.
23. Lan W, *et al.* (2018) Elucidating tricin-lignin structures: assigning correlations in HSQC spectra of monocot lignins. *Polymers (Basel)* 10(8):916.
24. Mansfield SD, Kim H, Lu F, & Ralph J (2012) Whole plant cell wall characterization using solution-state 2D NMR. *Nat Protoc* 7:1579.
25. Das A, *et al.* (2018) Lignin conversion to low-molecular-weight aromatics via an aerobic oxidation-hydrolysis sequence: comparison of different lignin sources. *ACS Sust Chem Eng* 6(3):3367-3374.
26. Salvachúa D, *et al.* (2016) Lignin depolymerization by fungal secretomes and a microbial sink. *Green Chem* 18:6046-6062.
27. Rencoret J, *et al.* (2018) A commercial laccase-mediator system to delignify and improve saccharification of the fast-growing *Paulownia fortunei* (Seem.) Hemsl. *Holzforschung* 73(1):45-54.
28. Ahmad M, *et al.* (2011) Identification of DypB from *Rhodococcus jostii* RHA1 as a lignin peroxidase. *Biochem* 50(23):5096-5107.
29. Santos A, Mendes S, Brissos V, & Martins LO (2014) New dye-decolorizing peroxidases from *Bacillus subtilis* and *Pseudomonas putida* MET94: towards biotechnological applications. *Appl Microbiol Biotechnol* 98(5):2053-2065.
30. Brown ME, Barros T, & Chang MC (2012) Identification and characterization of a multifunctional dye peroxidase from a lignin-reactive bacterium. *ACS Chem Biol* 7(12):2074-2081.
31. Granja-Travez RS & Bugg TDH (2018) Characterization of multicopper oxidase CopA from *Pseudomonas putida* KT2440 and *Pseudomonas fluorescens* Pf-5: Involvement in bacterial lignin oxidation. *Arch Biochem Biophys* 660:97-107.
32. Majumdar S, *et al.* (2014) Roles of small laccases from *Streptomyces* in lignin degradation. *Biochem* 53(24):4047-4058.
33. Misal SA & Gawai KR (2018) Azoreductase: a key player of xenobiotic metabolism. *Bioresour Bioproc* 5:17.
34. Gonçalves AM, Mendes S, de Sanctis D, Martins LO, & Bento I (2013) The crystal structure of *Pseudomonas putida* azoreductase - the active site revisited. *FEBS J* 280(24):6643-6657.
35. Griese JJ, P. Jakob R, Schwarzingler S, & Dobbek H (2006) Xenobiotic reductase A in the degradation of quinoline by *Pseudomonas putida* 86: physiological function, structure and mechanism of 8-hydroxycoumarin reduction. *J Mol Biol* 361(1):140-152.
36. Widiatnigrum T, Maeda S, Kataoka K, & Sakurai T (2015) A pirin-like protein from *Pseudomonas stutzeri* and its quercetinase activity. *Biochem Biophys Res* 3:144-149.
37. Lario PI, Sampson N, & Vrielink A (2003) Sub-atomic resolution crystal structure of cholesterol oxidase: what atomic resolution crystallography reveals about enzyme mechanism and the role of the FAD cofactor in redox activity. *J Mol Biol* 326(5):1635-1650.
38. Greule A, Stok JE, De Voss JJ, & Cryle MJ (2018) Unrivalled diversity: the many roles and reactions of bacterial cytochromes P450 in secondary metabolism. *Nat Prod Rep* 35(8):757-791.
39. Martínez AT, *et al.* (2017) Oxidoreductases on their way to industrial biotransformations. *Biotechnol Adv* 35(6):815-831.
40. Bendtsen JD, Nielsen H, Widdick D, Palmer T, & Brunak S (2005) Prediction of twin-arginine signal peptides. *BMC Bioinformatics* 6:167.
41. Petersen TN, Brunak S, von Heijne G, & Nielsen H (2011) SignalP 4.0: discriminating signal peptides from transmembrane regions. *Nat methods* 8:785.
42. Bendtsen JD, Kiemer L, Fausbøll A, & Brunak S (2005) Non-classical protein secretion in bacteria. *BMC Microbiol* 5(1):58.
43. Yu NY, *et al.* (2010) PSORTb 3.0: improved protein subcellular localization prediction with refined localization subcategories and predictive capabilities for all prokaryotes. *Bioinformatics (Oxford, England)* 26(13):1608-1615.
44. Choi CW, *et al.* (2014) Proteomic characterization of the outer membrane vesicle of *Pseudomonas putida* KT2440. *J Proteome Res* 13(10):4298-4309.
45. McMahon KJ, Castelli ME, Garcia Vescovi E, & Feldman MF (2012) Biogenesis of outer membrane vesicles in *Serratia marcescens* is thermoregulated and can be induced by activation of the Rcs phosphorelay system. *J Bacteriol* 194:3241-3249.
46. Bonnington KE & Kuehn MJ (2014) Protein selection and export via outer membrane vesicles. *Biochim Biophys Acta* 1843:1612-1619.
47. Baumgarten T, *et al.* (2012) Membrane vesicle formation as a multiple-stress response mechanism enhances *Pseudomonas putida* DOT-T1E cell surface hydrophobicity and biofilm formation. *Appl Environm Microbiol* 78:6217-6224.
48. Marisa Heredia R, *et al.* (2016) Release of outer membrane vesicles in *Pseudomonas putida* as a response to stress caused by cationic surfactants. *Microbiol* 162:813-822.
49. Tashiro Y, *et al.* (2017) Interaction of bacterial membrane vesicles with specific species and their potential for delivery to target cells. *Front Microbiol* 8(571).
50. O'Donoghue EJ & Krachler AM (2016) Mechanisms of outer membrane vesicle entry into host cells. *Cellular Microb* 18(11):1508-1517.
51. Gómez-Toribio V, García-Martín AB, Martínez MJ, Martínez ÁT, & Guillén F (2009) Induction of extracellular hydroxyl radical production by white-rot fungi through quinone redox cycling. *Appl Environm Microbiol* 75(12):3944.
52. Lee WD, Mukha D, Aizenshtein E, & Shlomi T (2019) Spatial-fluxomics provides a subcellular-compartmentalized view of reductive glutamine metabolism in cancer cells. *Nat Commun* 10(1):1351.
53. Achreja A, *et al.* (2017) Exo-MFA - A ¹³C metabolic flux analysis framework to dissect tumor microenvironment-secreted exosome contributions towards cancer cell metabolism. *Metab Eng* 43(Pt B):156-172.
54. Zhang H, *et al.* (2018) Identification of distinct nanoparticles and subsets of extracellular vesicles by asymmetric flow field-flow fractionation. *Nat Cell Biol* 20(3):332-343.
55. Salvachúa D, *et al.* (2018) Bioprocess development for muconic acid production from aromatic compounds and lignin. *Green Chem* 20(21):5007-5019.
56. Belda E, *et al.* (2016) The revisited genome of *Pseudomonas putida* KT2440 enlightens its value as a robust metabolic chassis. *Environm Microbiol* 18(10):3403-3424.

57. Nikel PI & de Lorenzo V (2018) *Pseudomonas putida* as a functional chassis for industrial biocatalysis: From native biochemistry to trans-metabolism. *Metab Eng* 50:142-155.
58. Clarke PH (1982) The metabolic versatility of pseudomonads. *Antonie van Leeuwenhoek* 48(2):105-130.
59. Calero P, et al. (2018) Genome-wide identification of tolerance mechanisms toward *p*-coumaric acid in *Pseudomonas putida*. *Biotechnol Bioeng* 115(3):762-774.
60. Dvořák P, Nikel PI, Damborský J, & de Lorenzo V (2017) Bioremediation 3.0: Engineering pollutant-removing bacteria in the times of systemic biology. *Biotechnol Adv* 35(7):845-866.
61. Nikel PI, Martínez-García E, & de Lorenzo V (2014) Biotechnological domestication of pseudomonads using synthetic biology. *Nat Rev Microbiol* 12(5):368-379.
62. Alves NJ, et al. (2015) Bacterial Nanobioreactors--Directing Enzyme Packaging into Bacterial Outer Membrane Vesicles. *ACS Appl Mater Interfaces* 7(44):24963-24972.
63. Behrendorff JBYH, Borràs-Gas G, & Pribil M (2019) Synthetic protein scaffolding at biological membranes. *Trends Biotechnol.*
64. Alves NJ, Turner KB, Medintz IL, & Walper SA (2016) Protecting enzymatic function through directed packaging into bacterial outer membrane vesicles. *Sci Rep* 6:24866.
65. Bomberger JM, et al. (2009) Long-distance delivery of bacterial virulence factors by *Pseudomonas aeruginosa* outer membrane vesicles. *PLoS pathogens* 5:e1000382.
66. de Paula RG, et al. (2019) Extracellular vesicles carry cellulases in the industrial fungus *Trichoderma reesei*. *Biotechnol Biofuel* 12:146-146.
67. Arntzen MØ, Várnai A, Mackie RI, Eijssink VGH, & Pope PB (2017) Outer membrane vesicles from *Fibrobacter succinogenes* S85 contain an array of carbohydrate-active enzymes with versatile polysaccharide-degrading capacity. *Environm Microbiol* 19(7):2701-2714.
68. Ichikawa S, et al. (2019) Cellulosomes localise on the surface of membrane vesicles from the cellulolytic bacterium *Clostridium thermocellum*. *FEMS Microbiol Lett* 366(12).
69. Jha RK, et al. (2018) A protocatechuate biosensor for *Pseudomonas putida* KT2440 via promoter and protein evolution. *Metab Eng Comm* 6:33-38.
70. Sluiter A, et al. (2006) Determination of sugars, byproducts, and degradation products in liquid fraction process samples. *NREL Laboratory Analytical Procedure.*
71. Karp EM, et al. (2018) Post-fermentation recovery of biobased carboxylic acids. *ACS Sust Chem Eng* 6(11):15273-15283.
72. Wessel D & Flugge UI (1984) A method for the quantitative recovery of protein in dilute solution in the presence of detergents and lipids. *Anal Biochem* 138(1):141-143.